

A general method for active surface adjustment of cable net structures with smart actuators

Zuowei Wang and Tuanjie Li*

*School of Electromechanical Engineering, Xidian University, 2 South Taibai Road,
Xi'an, Shaanxi 710071, China*

(Received March 21, 2014, Revised June 16, 2014, Accepted July 7, 2014)

Abstract. Active surface adjustment of cable net structures is becoming significant when large-size cable net structures are widely applied in various fields, especially in satellite antennas. A general-duty adjustment method based on active cables is proposed to achieve active surface adjustment or surface profile reconfiguration of cable net structures. Piezoelectric actuators and voice coil actuators are selected for constructing active cable structures and their simplified mechanical models are proposed. A bilevel optimization model of active surface adjustment is proposed based on the nonlinear static model established by the direct stiffness method. A pattern search algorithm combined with the trust region method is developed to solve this optimization problem. Numerical examples of a parabolic cable net reflector are analyzed and different distribution types of active cables are compared.

Keywords: active surface adjustment; cable net structure; smart actuator; direct stiffness method; pattern search algorithm

1. Introduction

A variety of space structure forms were born to adapt to harsh space environments and accomplish special space missions. Among these structure forms, cable net structures are a large class of critical structures currently being developed and planned to achieve various missions of spacecrafts. Representative structures include deployable mesh reflector antennas and large diameter space radio telescopes. They have been widely applied in the fields of satellite communications, earth observations, land remote sensing and deep space explorations. Examples include many renowned projects, such as ETS-VIII (Meguro *et al.* 2009), THURAYA 1-3 (Thomson 2002), MUSES-B (Natori *et al.* 1993), “NEXRAD in Space” and GEO-mobile satellites.

The increasing interests of cable net structures for space applications have led to the growing demands for high surface accuracy and large size (Thomson 2002). These demands have great effects on performances of space explorations. For mesh reflector antennas, large diameter and high precision reflectors not only are capable of transmitting greater amount of data with higher resolution, but also can expand their working frequency bandwidth from S-band to Ku-band or

*Corresponding author, Professor, E-mail: tjli888@126.com

Ka-band (Li and Wang 2009). However, large-size cable net structures easily suffer from the effects of particular surroundings, such as plasma, particle, radiative outputs from the sun, and high and low temperature alternation. These environmental factors will deteriorate surface accuracy of cable net structures in turn. Furthermore, space cable net structures are required to be surface reconfiguration in order to achieve a variety of space missions. Therefore, how to maintain and adjust the surface profile of space cable net structures to satisfy performance requirements is extremely pivotal and challengeable in further space applications.

Cable net structures belong to the family of flexible tension structures characterized by strong geometric nonlinearities. Cable net structures become stiffer as the deformation of cables increases, as long as they remain in tension. The initial stiffness of these structures is determined by cable tension forces. The tension forces must be high enough to avoid slackening cables under various load combinations, because in that case the cable net structure becomes soft and may undergo large deformations (Vassilopoulou and Gantes2010). The shape of cable net structures depends on the prestress distribution in cables, and the prestresses are coupled (Wang *et al.* 2013). Therefore, a little variation of the geometrical shape of flexible cable net structures may result in a large variation of structural behaviors.

Some shape control methods of cable net structures have recently been investigated. The displacement control scheme of prestressed cable-strut structures by actuating some structural members was proposed by You (1997). The proposed method is only appropriate for the case of small deformation of linearly elastic materials, which does not consider the geometric nonlinearity of cables and the actuation mechanism. A shape adjustment algorithm of flexible antenna reflectors is explored through altering the sensitivity matrix of the adjustment cable length to the surface displacements (Tabata *et al.* 1992). However, the sensitivity matrix needs to be ceaselessly re-calculated corresponding to the change of surface shape, which is difficult to be achieved in orbit. Some shape control algorithms of space mesh reflectors based on the force density method have been investigated by two ways (Tanaka 2013): boundary cables of front cable net which is attached to deployable truss assembly and tension tie cables. In these studies, the proposed methods only can be applied to the design stage or ground adjustment of cable net reflectors, which is large workload as the diameter increases. Feasibility of active shape formation or correction of a tension truss antenna (TTA) under the conditions of limited number of actuators and limited information of its surface shape is researched (Tabata and Natori1996). However, the effects of actuators on structural behaviors are not taken into account. Active shape control of mesh reflectors using piezoelectric (PZT) actuators has been addressed in the literature (Wang *et al.* 2014). In these papers, the active adjustment algorithm is on the basis of the finite element method, which is limited by actuators and the distribution of active cables.

The main purpose of this paper is to propose a general-duty active surface adjustment method based on the direct stiffness method, which can analyze active cable structures with different smart actuators and different distributions of active cables. The active cable structure incorporates a smart actuator into two flexible cables. It can realize the stress redistribution of cable net structures by slightly lengthening or shortening the adjustment cables. The active cable structure provides a way for active surface control and profile reconfiguration of space cable net structures.

This paper is organized as follows. First, the description of cable net structure with active cables is presented in Section 2. Then, the general-duty analysis model of cable net structures with active cables is established in Section 3. In the following, the active surface adjustment method is proposed in Section 4. Next, in Section 5, numerical simulations of the cable net reflector are illustrated. Finally, some conclusions are outlined in Section 6.

2. Description of active cable structures

The active cable structure consists of a smart actuator and two cables with the same parameters, as shown in Fig. 1. D_i and D_j are the displacement of node i and j , respectively. The actuators are constructed by the internal actuation part and external connecting sleeve. The actuation part produces large actuation force when voltages are applied to them. As a result, the change of force in active cable may result in the stress redistribution of the whole cable net structure. Therefore, the active cable structure is a good candidate for active shape control of cable net structures, especially space mesh antennas.

2.1 Selection of actuators

The selection of actuators is limited by space applications and demands of active surface adjustment. The actuators require low power consumption, small volume, light weight, high reliability, no electromagnetic interference and large output force or output displacement. To satisfy these requirements, PZT actuators and voice coil actuators (VCAs) are discussed in this section.

2.1.1 PZT actuators

According to the inverse piezoelectric effect, PZT actuators induce an expansion of the material to produce a large output force. There are different types of PZT actuators such as stack and bending types, etc. As the stack type enables very high output forces, it is selected to actively adjust the surface profile of cable net structures.

Using the notations of the IEEE standard on piezoelectricity (Kaltenbacher *et al.* 2010), the constitutive equations of a one-dimensional piezoelectric material are

$$\begin{Bmatrix} D \\ l \end{Bmatrix} = \begin{bmatrix} \sigma^T(1-c^2) & d_{33}/s^E \\ -d_{33}/s^E & 1/s^E \end{bmatrix} \begin{Bmatrix} E \\ S \end{Bmatrix} \quad (1)$$

where D is the electric displacement, E is electric intensity, l is the stress, and S is the strain. σ^T is the dielectric constant (permittivity) under the constant stress, s^E is the compliance constant when the electric field is constant (inverse of the Young's modulus), and d_{33} is the piezoelectric constant. The reason for the subscript 33 is that, index 3 is always aligned to the poling direction of the material, and the electric field is assumed to be parallel to the poling direction. c is the electromechanical coupling factor.

If all electrical and mechanical quantities are assumed to be uniformly distributed, the constitutive equations of the PZT stack formed by n disks with the cross section area of A_p , as shown in Fig. 2(a), can be obtained by integrating Eq. (1) (Preumont 2002).

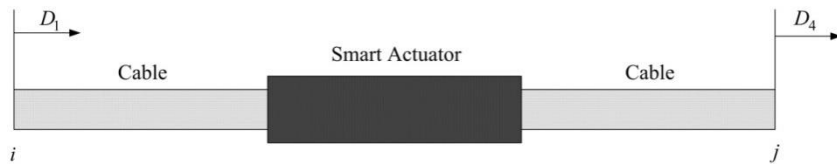


Fig. 1 Schematic diagram of active cable structures

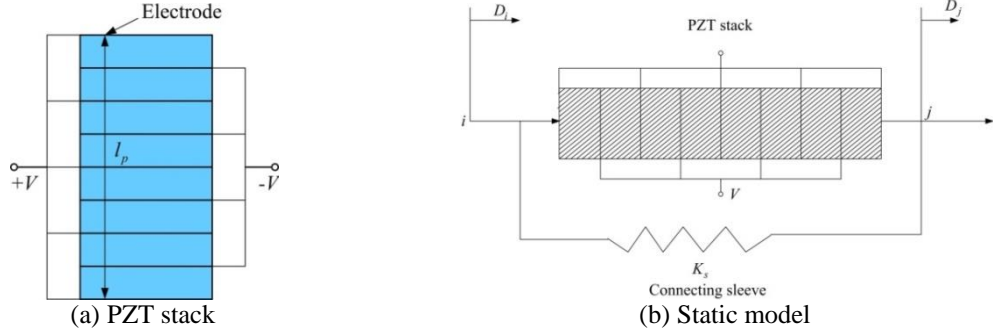


Fig. 2 Actuation principle of PZT actuators

$$\begin{Bmatrix} Q \\ f_p \end{Bmatrix} = \begin{bmatrix} C(1-\gamma^2) & nd_{33}K_p \\ -nd_{33}K_p & K_p \end{bmatrix} \begin{Bmatrix} V \\ \Delta \end{Bmatrix} \quad (2)$$

where, Q is the total electric charge on the electrodes of PZT stack, Δ is the total extension, f_p is the total force, C is the capacitance, and V is the voltage applied between the electrodes of PZT stack. γ is the electromechanical coupling factor of the material, which measures the efficiency of the conversion of mechanical energy into electrical energy. $K_p = A_p / (l_p S^E)$ is the stiffness with short-circuited electrodes ($V = 0$) and l_p is the length of PZT stack.

According to the mechanical behaviors of PZT actuators, the one-dimensional static model of PZT actuators is proposed in Fig. 2(b), where K_s denotes the stiffness of the external connecting sleeve. According to Eq. (2), the member force of PZT actuators can be given as

$$N = -nd_{33}K_p V + (K_p + K_s)\Delta \quad (3)$$

where $\Delta = D_j - D_i$.

2.1.2 Voice coil actuators

VCAs are a type of ideal linear actuators as its output force is almost constant. The electromagnetic force of VCAs is generated by the moving coil cutting the magnetic field of a permanent magnet. The force produced by VCAs is proportional to the applied current I through the coil and can be expressed by (Preumont 2002)

$$f_{VCA} = K_{VCA} I \quad (4)$$

where K_{VCA} is the force constant determined by the magnetic induction flux density and the number of wire turns of VCAs.

The circuit diagram for generating the electromagnetic force is shown in Fig. 3(a). In the circuit, V is the voltage at the output of the power amplifier, R is the electrical resistance of the coils, v is the velocity and E_V is the back electromotive force. The slight coil inductance and capacitance are ignored. Summing the voltages around the circuit of Fig. 3(a) yields

$$-V + IR + E_V = 0 \quad (5)$$

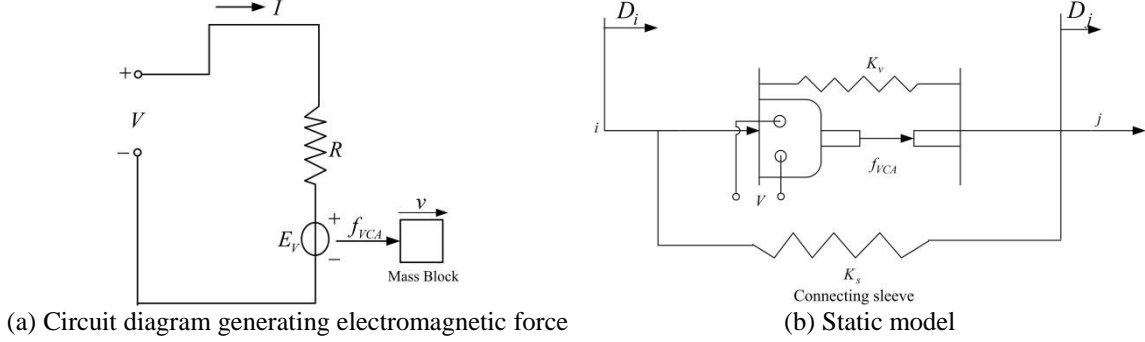


Fig. 3 Actuation principle of VCAs

Substituting Eq. (5) into Eq. (4) allows us to determine the voice coil force which acts on the mass block as follows.

$$f_{VCA} = \frac{K_{VCA}V}{R} - \frac{K_{VCA}^2v}{R} \quad (6)$$

The voice coil force is almost proportional to V as the velocity of VCAs is slight. In order to integrate with cables easily, a simple static model of VCAs is proposed in Fig. 3(b). The member force can then be described as

$$N = \frac{K_{VCA}V}{R} + (K_v + K_s)\Delta \quad (7)$$

where K_v is the stiffness of the internal actuation part.

Compared to a PZT actuator, the VCA, in general, needs a larger voltage for generating the same actuation force. In order to integrate actuators with cables, the canonical form of Eqs. (3) and (7) is required. M and k_2 are respectively denoted as the force coefficient and stiffness coefficient: for PZT actuators, $k_2=K_p+K_s$ and $M=-nd_{33}K_p$; for VCAs, $k_2=K_v+K_s$ and $M = K_{VCA}/R$. The unified formulation of the member force is given by

$$N = MV + k_2\Delta \quad (8)$$

2.2 Model of active cables

The active cable shown in Fig. 1 can be equivalent to three springs in series. By the displacement superposition principle, it yields

$$\frac{N}{k_1} + \frac{N - MV}{k_2} + \frac{N}{k_1} = \Delta \quad (9)$$

with

$$k_1 = E_c A_c / L_c \quad (10)$$

where A_c , E_c and L_c are the cross section area, elastic modulus and length of cables respectively. $\Delta = D_j - D_i$ is the displacement of the whole active cable. By Eq. (9), the member force of the whole active cable can be rewritten as

$$N = \frac{k_1^2 k_2}{K_1} \Delta + \frac{k_1^2}{K_1} MV \quad (11)$$

where $K_1 = k_1^2 + 2k_1 k_2$. It can be noted from Eq. (11) that the member force of active cables is the sum of the elastic force and actuation force. In order to model the whole cable net reflector simply, an equivalent relation is introduced

$$\frac{k_1^2 k_2}{K_1} = \frac{E_{act} A_{act}}{L_{act}} \quad (12)$$

with

$$L_{act} = 2L_c + L_a, A_{act} = A_c \quad (13)$$

where E_{act} , A_{act} and L_{act} are the elastic modulus, cross sectional area, length of active cables, respectively. L_a is the length of actuators. E_{act} can be easily determined by Eqs. (12) and (13). Then, the member force of active cables can be further given by

$$N = \frac{E_{act} A_{act}}{L_{act}} \Delta + \frac{k_1^2}{K_1} MV \quad (14)$$

3. Nonlinear static analysis

In this section, the direct stiffness method is developed for the nonlinear static analysis of cable net structures with smart actuators. The cables of the active cable net structure can be divided into two types: passive cables without actuators and active cables with actuators. As the following derivation is common for the both passive cable members and active cable members, the subscripts denoting them are omitted for simple.

3.1 Static model

The undeformed and deformed configurations of the cable member are shown in Fig. 4 with nodes i and j as its two ends. These nodes before deformation can be described by the position vectors \vec{R}_i and \vec{R}_j . Then, the unit vector in the longitudinal direction of the cable member before deformation is

$$\vec{\alpha} = \frac{1}{\|\vec{L}\|} \vec{L} = \alpha_x \vec{e}_1 + \alpha_y \vec{e}_2 + \alpha_z \vec{e}_3 \quad (15)$$

with

$$\vec{L} = \vec{R}_j - \vec{R}_i$$

where $\vec{e}_1, \vec{e}_2, \vec{e}_3$ are the unit vectors of the global coordinate system xyz , and $\alpha_x, \alpha_y, \alpha_z$ are the direction cosines of the cable member undeformed.

The position vectors of nodes i and j after the deformation can be described as

$$\vec{r}_i = \vec{R}_i + \vec{D}_i, \vec{r}_j = \vec{R}_j + \vec{D}_j \quad (16)$$

Then, the unit vector in the longitudinal direction of the deformed member is

$$\vec{\beta} = \frac{1}{\|\vec{\rho}\|} \vec{\rho} = \beta_x \vec{e}_1 + \beta_y \vec{e}_2 + \beta_z \vec{e}_3 \quad (17)$$

with

$$\vec{\rho} = \vec{r}_j - \vec{r}_i$$

where $\beta_x, \beta_y, \beta_z$ are the direction cosines of the cable member after the deformation.

The elongation of the cable member undergoing deformation is

$$\Delta L = \vec{\rho} \cdot \vec{\beta} - \vec{L} \cdot \vec{\alpha} = (\vec{\beta} - \vec{\alpha}) \vec{L} + (\vec{D}_j - \vec{D}_i) \vec{\beta} \quad (18)$$

By Eqs. (15)-(18), it is easily to found

$$\Delta L = [-1 \quad 1] [T_\beta] \{D_m\} + u \quad (19)$$

where

$$\begin{aligned} \{D_m\} &= (D_{xi}, D_{yi}, D_{zi}, D_{xj}, D_{yj}, D_{zj})^T \\ [T_\beta] &= \begin{bmatrix} \beta_x & \beta_y & \beta_z & 0 & 0 & 0 \\ 0 & 0 & 0 & \beta_x & \beta_y & \beta_z \end{bmatrix} \\ u &= [-1 \quad 1] \begin{bmatrix} \alpha_x & \alpha_y & \alpha_z \\ \beta_x & \beta_y & \beta_z \end{bmatrix} \begin{bmatrix} L_x \\ L_y \\ L_z \end{bmatrix} \end{aligned}$$

Based on the assumption of linearly elastic materials and small strain, the member force can be expressed by

$$N = EA \frac{\Delta L}{L} \equiv \frac{EA}{L} [-1 \quad 1] [T_\beta] \{D_m\} + \frac{EA}{L} u + f_{act} \quad (20)$$

where $f_{act} = 0$ for passive cable members and $f_{act} = MVk_1^2 / K_1$ for active cable members.

By coordinate transformation, the nodal forces of cable members in the global coordinates xyz are obtained as

$$\{Q_e\} = [k_e] \{D_m\} + \{U_e\} + \{f_{act,e}\} \quad (21)$$

where

$$\begin{bmatrix} \mathcal{K}_e^0 \\ \mathcal{K}_e^1 \end{bmatrix} = \frac{EA}{L} \begin{bmatrix} 1 & -1 \\ -1 & 1 \end{bmatrix}, [k_e] = [T_\beta]^{-T} \begin{bmatrix} \mathcal{K}_e^0 \\ \mathcal{K}_e^1 \end{bmatrix} [T_\beta] \quad (22)$$

$$\{U_e\} = [T_\beta]^{-T} \begin{bmatrix} \mathcal{K}_e^0 \\ \mathcal{K}_e^1 \end{bmatrix} \begin{bmatrix} \alpha_x & \alpha_y & \alpha_z \\ \beta_x & \beta_y & \beta_z \end{bmatrix} \begin{bmatrix} L_x \\ L_y \\ L_z \end{bmatrix}, \{f_{act,e}\} = [T_\beta]^{-T} \begin{Bmatrix} -1 \\ 1 \end{Bmatrix} f_{act} \quad (23)$$

Assembling Eq. (21) at all cable members forms the global equilibrium equation

$$[K_{NL}]\{D_{def}\} + \{U\} = \{Q\} - \{f_{act}\} \quad (24)$$

where $\{D_{def}\}$ is the global nodal displacement vector, $\{Q\}$ is the external force vector including the temperature load and $\{f_{act}\}$ is the actuation force vector. The $\{U\}$ and $[K_{NL}]$ are assembled from $[k_e]$ and $\{U_e\}$, which are the function of the undeformed profile.

3.2 Algorithm of solving the nonlinear model

The nonlinear problem Eq. (24) is transformed into a unconstraint optimization problem

$$\text{Min } F = \frac{1}{2} \|[K_{NL}]\{D_{def}\} + \{U\} - \{Q\} + \{f_{act}\}\|^2 \quad (25)$$

For solving the nonlinear optimization problem like Eq. (25), the trust region method and linear search method are two classes of main numerical methods (Kettil and Wiberg 2004). Compared to the linear search method, the trust region method has high reliability and strong global convergence property. The most important point is that the trust region method can deal with relaxation problem of cables. Thus, the trust region method is used in the paper.

The updating policy of trust region radius was suggested by Nocedal and Wright (2006). The unspecified sub-optimization problem of Eq. (25) in the each iteration is

$$\text{Min } F_j(\{D_{def}\}_j) + \{g_D\}_j \{p_D\} + \frac{1}{2} \{p_D\}^T [\nabla^2 F_j(\{D_{def}\}_j)] \{p_D\} \quad (26)$$

where $\{p_D\}$ is the solution of sub-optimization problem, $\{g_D\}_j$ is the gradient function, and the term of $[\nabla^2 F_j(\{D_{def}\}_j)]$ is the Hessian matrix in the iteration j . The gradient function at each step can be obtained by

$$\begin{aligned} \{g_D\}_j &= dF_j(\{D_{def}\}_j) / d\{D_{def}\}_j^T \\ &= (\{D_{def}\}_j^T [K_{NL}]^T + \{U\}^T + \{f_{act}\}^T - \{Q\}^T) [J_{def,D}]_j \end{aligned} \quad (27)$$

with

$$[J_{def,D}]_j = d\{[K_{NL}]\{D_{def}\} + \{U\} + \{f_{act}\}\}_j / d\{D_{def}\}_j^T \quad (28)$$

where $[J_{def,D}]_j$ is the Jacobian matrix of cable net structures. It can be linearly assembled from the local Jacobian matrix derived from Eq.(20), which was discussed in the reference (Shi and Yang 2012).

As cable forces must be not less than 0, a nonlinear elastic modulus for both cable members and active cable members is introduced for the nonlinear solution algorithm.

$$E(\delta) = \begin{cases} E_c \text{ or } E_{act}, & \delta > 0 \\ 0, & \delta \leq 0 \end{cases} \quad (29)$$

where δ is cable strain.

The Hessian approximation is applied to reduce the calculated amount (Shultz *et al.*1985).

$$[B_D]_j = [J_{def,D}]_j^T [J_{def,D}]_j \approx \nabla^2 F_j(\{D_{def}\}_j) \quad (30)$$

Using Eqs. (26)-(30), the final cost function is revised when $F_j(\{D_{def}\}_j)$ is constant.

$$M_D(\{p_D\}) = \{g_D\}_j \{p_D\} + \frac{1}{2} \{p_D\}^T [\nabla^2 F_j(\{D_{def}\}_j)] \{p_D\} \quad (31)$$

The global solution of the trust region problem for each step can be concluded according to the following four cases (Shi and Yang 2012): when $[B_D]_j$ is positive definite and $\|-[B_D]_j^{-1} \{g_D\}_j^T\| \leq \pi$, where π is the trust region radius in each step; when $[B_D]_j$ is positive definite and $\|-[B_D]_j^{-1} \{g_D\}_j^T\| > \pi$; when $[B_D]_j$ is indefinite and $\{g_D\}_j \{q_1\} \neq 0$ where $\{q_1\}$ is the eigenvector corresponding to the smallest eigenvalue λ_1 , or when $[B_D]_j$ is indefinite, $\{g_D\}_j \{q_1\} = 0$ and $\|-([B_D]_j + \lambda_1 [I])^{-1} \{g_D\}_j^T\| \geq \pi$; when $[B_D]_j$ is indefinite and $\|-([B_D]_j + \lambda_1 [I])^{-1} \{g_D\}_j^T\| < \pi$.

4. Active surface adjustment analysis

The main purpose of surface adjustment is to achieve the desired profile from the current profile of cable net structures. The current profile can be obtained by digital measurement or nonlinear analysis model Eq. (24) from a known profile.

4.1 Surface adjustment model

The basic principle of active surface adjustment is that when a set of voltages are given, the generating unbalance actuation force, $\{f_{act}\}$, will make the cable net structure deformed. The surface root mean square (RMS) is used to evaluate the degree of approximation of the adjusted profile and desired profile. Then, the active surface adjustment model is expressed by

$$\begin{aligned} & \text{Find } \mathbf{V} = [V_1 \ \cdots \ V_i \ \cdots \ V_{r_a}]^T \\ & \text{Min } RMS = \sqrt{\left(\sum_{i=1}^m (\Delta x_i^2 + \Delta y_i^2 + \Delta z_i^2) \right) / m} \end{aligned} \quad (32a)$$

$$S.T. \ V_i \in [V^l, \ V^h] \ (i=1,2,\dots,r_a) \ \text{Min } F = \frac{1}{2} \left\| [K_{NL}] \{D_{def}\} + \{U\} - \{Q\} + \{f_{act}\} \right\|^2 \quad (32b)$$

where m is the number of nodes to evaluate RMS , r_a is the number of active cables, and V_j is the actuation voltage of the i active cable. V^h and V^l are the upper limit and lower limit of actuation voltages, respectively. Δx_i , Δy_i , and Δz_i are the position errors of the i th evaluation node in the directions of x , y , and z axis, respectively.

Eq. (32) is a typical bilevel nonlinear optimization problem. In view of its hierarchical relationship, Eq. (32(a)) is called the upper-level programming problem, while Eq. (32(b)) corresponds to the lower-level programming problem.

4.2 Solving method

A linear search method, pattern search algorithm (PS), is applied to solve the upper-level programming problem. The lower-level programming problem can be solved by the trust region method. The pattern search algorithm is an evolutionary technique that is suitable to solve a variety of optimization problems that lie outside the scope of the standard optimization methods and can be easily expanded to multidimensional cases (Breitkopf *et al.* 2005). Unlike other heuristic algorithms, such as genetic algorithms, PS possesses a flexible and well-balanced operator to enhance and adapt the global and fine tune local search.

The PS algorithm is started by establishing a set of points, called a mesh, around the given point which could be the initial starting point, $\mathbf{V}^{(0)}$, or computed from the previous step of the algorithm, $\mathbf{V}^{(best)}$. The mesh is formed by adding the current point to a scalar multiple of a set of vectors, called a pattern $\Delta \mathbf{V}$. The detailed solution processes of the multi dimensional PS algorithm are shown in Fig. 5, where k is the number of iteration steps. Two convergence conditions of surface adjustment must be satisfied: $|RMS^{(k-1)} - RMS^{(k)}| \leq \varepsilon$ for global optimal solution; $RMS^{(k)} \leq [RMS]$ for achieving RMS of engineering requirements.

5. Simulation examples

The cable net parabolic reflector, as shown in Fig. 6, is taken as an example to illustrate the proposed methods. The deployable cable net reflector is conceived with the concept of the tension truss, which is a light and inherently stiff structure that can be precisely and repeatedly deployed regardless of environment. As a central part of mesh reflector antennas, the cable net reflector can be divided into three parts: front cable net, back cable net and tension tie cables. The cables of front and back cable nets are composed by two types: boundary cables and surface cables. Front and back cable nets are both doubly curved geodesic nets that are placed back-to-back. Tension tie cables evenly apply equilibrium forces between front and back cable nets to preload them in

tension to maintain the surface profile of the reflector. The front cable net of the reflector is used to place the gold-plated molybdenum mesh surface to reflect RF communication. The peripheral nodes of front cable net are attached to the rigid supported truss (Thomson 2002). These peripheral nodes are assumed to be fixed in this paper.

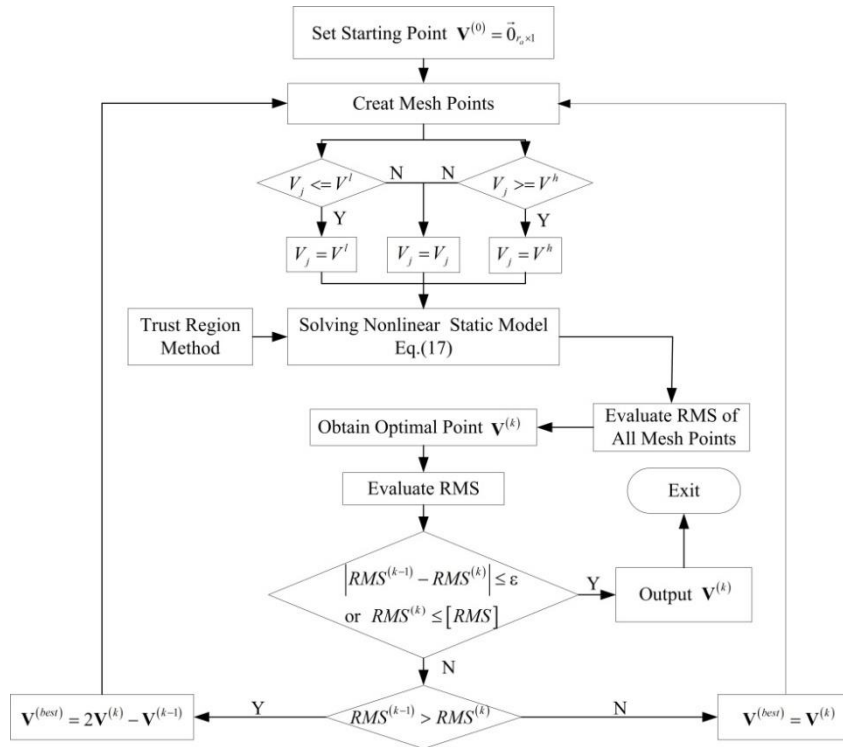


Fig. 5 Solution processes of the multidimensional PS algorithm

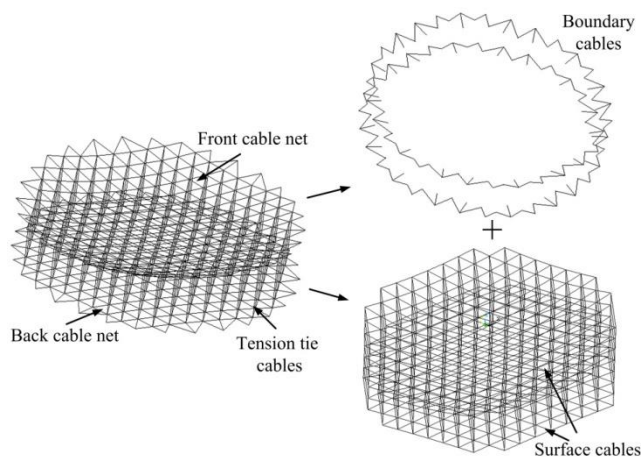


Fig. 6 Composition of cable net reflectors

Table 1 Material parameters of smart actuators

Item	PZT actuator	VCA
Cross-section area	$7.85 \times 10^{-4} \text{ m}^2$	$7.85 \times 10^{-4} \text{ m}^2$
Length L_a	0.1 m	0.1 m
Coil resistance R		2Ω
Force constant K_{VCA}		12 N/m^2
PZT disk n	100	
Elastic compliant coefficients ^E	$12 \times 10^{-12} \text{ m}^2/\text{N}$	
Piezoelectric strain constant d_{33}	$3.35 \times 10^{-8} \text{ m/V}$	
	$K_v + K_s \approx K_p + K_s = 2 \times 10^{11} \text{ N/m}^2$	

5.1 Model for analysis

All cables of the cable net reflector have the same material properties: the cross-sectional area of $1.956 \times 10^{-5} \text{ mm}^2$, the thermal expansion coefficient of $2 \times 10^{-6} \text{ m/}^\circ\text{C}$ and elastic modulus of $2 \times 10^{10} \text{ N/m}^2$. The properties of PZT actuators and VCAs are shown in Table 1.

Specifications of the parabolic reflector are given as follows.

Diameter of aperture: 5000 mm

Focal length of front cable net: 10000 mm

Focal length of back cable net: 60000 mm

Number of free nodes: 110

Number of fixed nodes: 60

Number of surface cables: 276

Number of boundary cables: 108

Number of tie cables: 55

Number of subdivisions: 8

Type of facet: triangular

Height: 500 mm

Required surface accuracy RMS of front cable net: $[\text{RMS}] = 0.35 \text{ mm}$

The active cables are used to adjust the surface accuracy of front cable net. Therefore, their placements must be directly related to the front cable net. Surface cables of front cable net placing the gold-plated molybdenum mesh is not suitable for placing actuators due to the intertwist problem of reflector deployment. In order to satisfy deployment reliability of reflector on-orbit, boundary cables of front cable net and tie cables are selected to place active cables. Three distribution types of active cables are proposed: (1) SYS-BOU, boundary cables of front cable net fully replaced by active cables; (2) SYS-TIE, tie cables fully replaced by active cables; (3) SYS-MIX, both the tie cables and boundary cables of front cable net partially replaced by active cables. The label of active cables of type SYS-TIE is shown in Fig. 7 according to their nodes

connected to front cable net. The labels of that of types SYS-BOU and SYS-MIX are shown in Figs. 8 and 9, respectively. The cable net reflector is deployed into a parabolic surface by the form-finding analysis with the tension mean value of 15 N in tie cables (Wang *et al.* 2014).

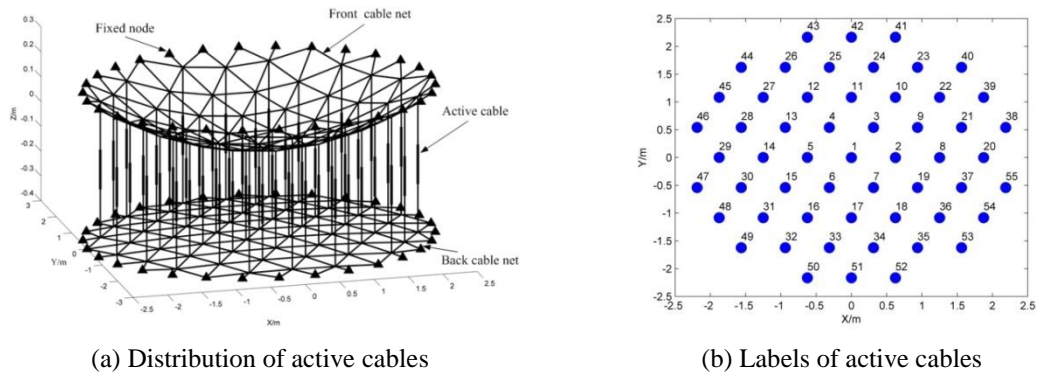


Fig. 7 Active cables of type SYS-TIE

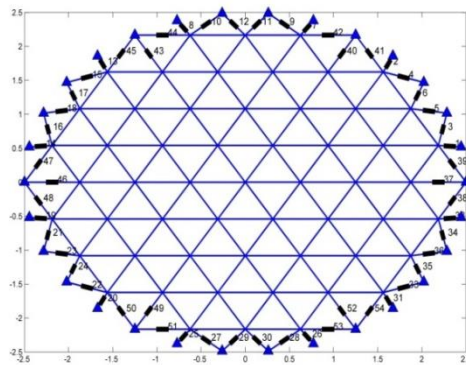


Fig. 8 Labels of active cables of type SYS-BOU

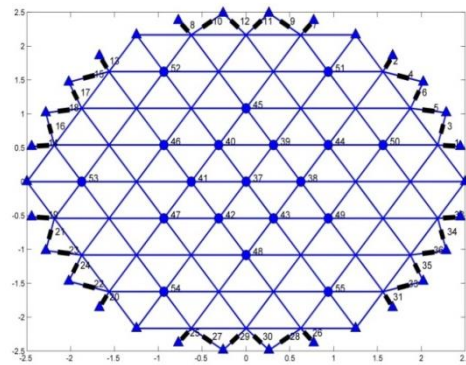


Fig. 9 Labels of active cables of type SYS-MIX

5.2 Results of active surface adjustment

5.2.1 Adjustment results with different actuators

A uniform temperature shift of -150°C are considered for modeling space temperature environment. The generated thermal strain is introduced into Eq. (19). The reflector profile after thermal deformations are determined by the nonlinear analysis based on Eq. (24). Surface error of front cable net is then shown in Fig. 10 with 2.36 mm RMS. The nodal displacement errors mainly distribute in reflector surface constructed by surface cables and the maximum nodal displacement of front cable net is 3.9 mm of the central node.

The distribution type SYS-TIE is used to evaluate the adjustment performance using different actuators. Two systems are constructed: system *I* using PZT actuators and system *II* using VCAs. The parameters for active profile adjustment are described as follows: (i) $k=12$; (ii) $V_j \in [-450\text{V}, 450\text{V}]$; (iii) $\Delta V_j = 3.57\text{V}$; (iv) $\varepsilon = 2 \times 10^{-6}$.

The iteration processes of RMS error of front cable net are depicted in Fig. 11. RMS error of system *I* drops drastically from 2.36 mm to 1.02 mm, and while that of system *II* ameliorates from 2.36 mm to 1.41 mm. It can be observed that the surface RMS error of cable net reflector with active cables is well improved by both PZT actuators and VCAs. The obtained surface accuracy of systems *I* and *II* are more than required RMS due to the limitations of actuation voltages and the number of iteration steps. The surface errors of front cable net are shown in Figs. 12 and 13. In these figures, nodal displacement errors of reflector surface constructed by surface cables are both improved. The displacement error of the central node decreases from 3.9 mm to 2.4 mm for system *I* and 2.8 mm for system *II*. All nodal displacement errors of the reflector illustrated in Fig. 12 are smaller than that in Fig. 13. Their optimal actuation voltages are shown in Fig. 14, which suggests that the maximum actuation voltage is 450V satisfying the limitation of actuation voltages. It can be noted that the obtained surface RMS error of system *I* is better than that of system *II*. This is because a PZT actuator provides the larger actuation force than a VCA when they are applied the same voltages. It expands the solution domain of active adjustment optimization model from the viewpoint of mathematics.

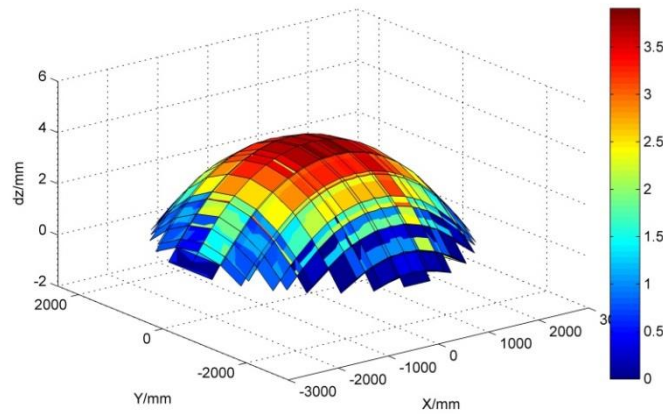


Fig. 10 Surface error of front cable net before active adjustment

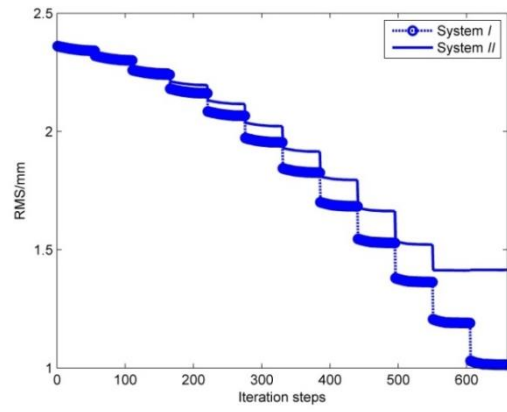


Fig. 11 Iteration processes of RMS error of systems *I* and *II*

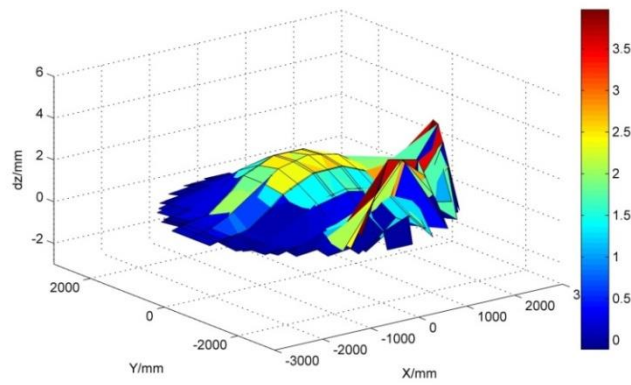


Fig. 12 Surface error of system *I* after active adjustment

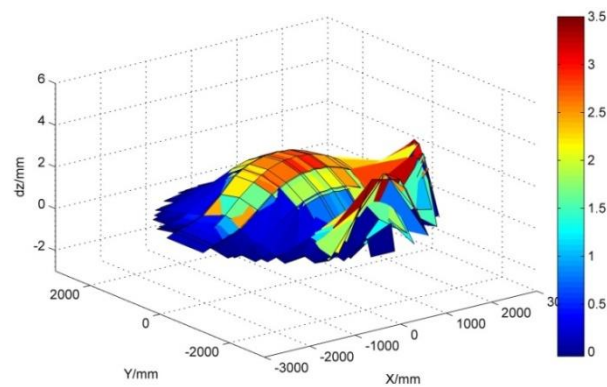


Fig. 13 Surface error of system *II* after active adjustment

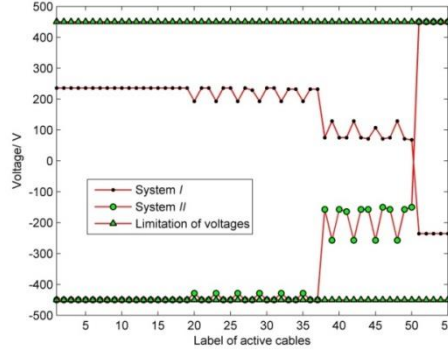


Fig. 14 Optimal actuation voltages of active profile adjustment

5.2.2 Adjustment results of different distribution types

Four different temperature conditions, shown in Table 2, are discussed in this section to compare adjustment performances using different distribution types. PZT actuators are used for the system. The parameters for active profile adjustment are described as: (i) $RMS < [RMS]$; (ii) $\Delta V_j = 3.57V$; (iii) $\varepsilon = 2 \times 10^{-6}$.

Adjustment results without the limitations of actuation voltages are summarized in Table 3. The obtained surface RMS for conditions *I* and *II* are slightly more than required RMS. It means that there may exist a precision limit for active surface adjustment of reflectors under given temperature loads. It can be noted from Table 3 that the adjusting effectiveness of type SYS-BOU is better than that of type SYS-TIE and the adjusting effect of type SYS-MIX is between them. This is because adjusting boundary cables will change global mechanical boundaries of the whole reflector while adjusting tension tie cables change only local boundaries of front and back cable nets. For type SYS-MIX, part of boundary cables are changed, which refers to the optimal allocation problem of actuators.

The optimal actuation voltages of three distribution types under temperature conditions *I*, *II*, *III* and *IV* are shown in Figs.15-18, respectively. It can be observed that the actuation voltages of types SYS-BOU and SYS-MIX are far less than that of type SYS-TIE. It comes into a conclusion that the actuators placed in boundary cables can consume less energy than that placed in tie cables for active surface adjustment. It can be also noted that actuation voltages of all types for condition *III* are smaller than that for condition *I*, and actuation voltages of all types for condition *IV* are smaller than that for condition *II*. This is because that the deformations of the unadjusted surface profile become larger due to larger temperature variations.

Table 2 Different temperature conditions

Item	Condition <i>I</i>	Condition <i>II</i>	Condition <i>III</i>	Condition <i>IV</i>
Uniform temperature shift	- 150°C	150°C	- 100°C	100°C

Table 3 Adjustment results using different distribution types

Item	RMS(mm)			
	Condition I	Condition II	Condition III	Condition IV
Before Adjustment	0.002361	0.002683	0.001597	0.001823
Type SYS-TIE	0.000368	0.000446	0.000295	0.000306
Type SYS-BOU	0.000319	0.000363	0.000206	0.000218
Type SYS-MIX	0.000362	0.000377	0.000229	0.000249

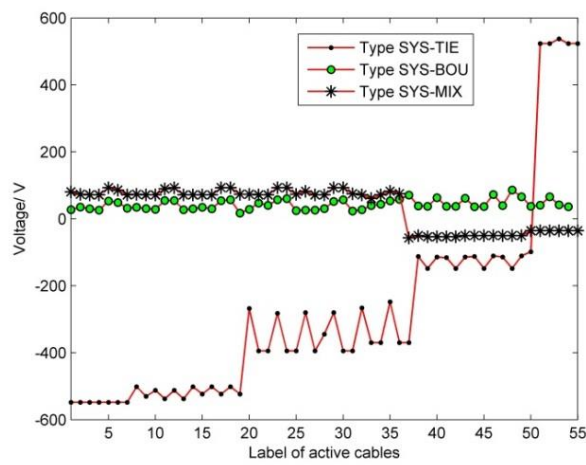


Fig. 15 Optimal actuation voltages of active surface adjustment under condition I

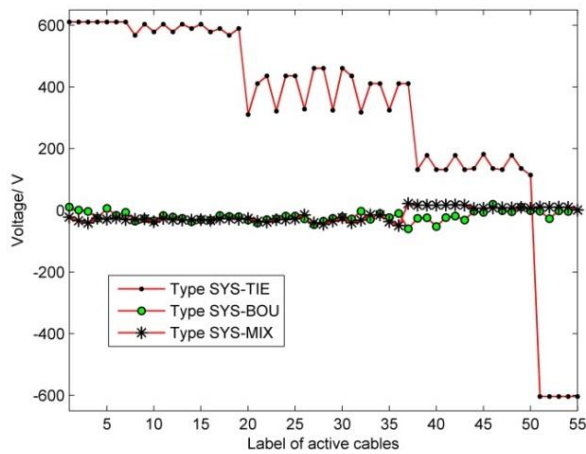


Fig. 16 Optimal actuation voltages of active surface adjustment under condition II

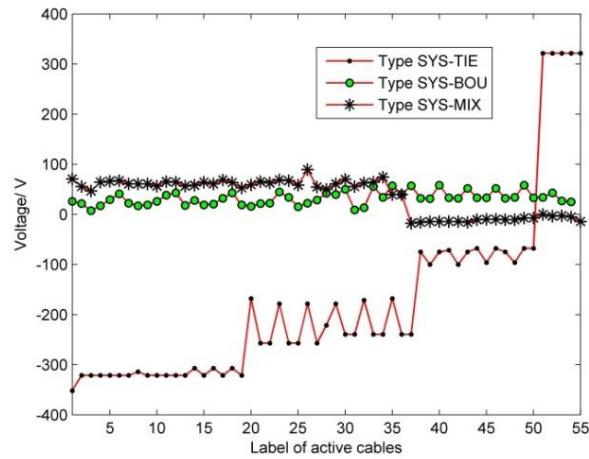


Fig. 17 Optimal actuation voltages of active surface adjustment under condition *III*

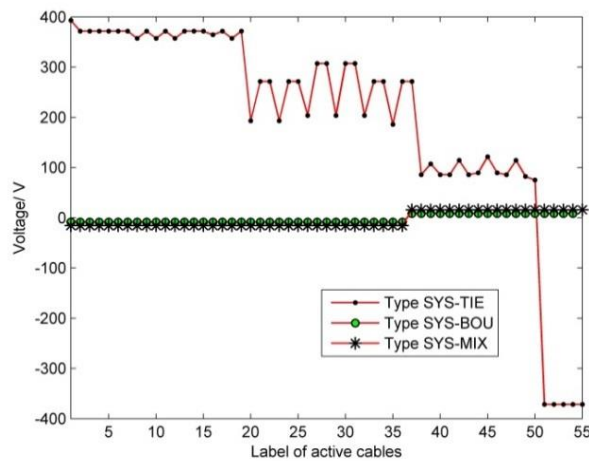


Fig. 18 Optimal actuation voltages of active surface adjustment under condition *IV*

6. Conclusions

This paper proposes a general-duty method for active surface adjustment of cable net structures based on active cable structures. Two types of linear actuators, PZT actuators and VCAs, are selected to construct the active cable structure. A general static analysis model is developed for active surface adjustment with different actuators. A parabolic cable net reflector is used to verify the validity of the proposed methods and adjustment performances of three distribution types of active cables are compared. Active surface adjustment using PZT actuators can achieve better RMS than surface adjustment using VCAs. The actuators placed in boundary cables need to be applied far less voltages than that placed in tie cables for achieving the desired surface profile.

Acknowledgments

The research described in this paper was financially supported by National Natural Science Foundation of China (Grant No. 51375360) and the Fundamental Research Funds for the Central Universities (No.K505131000087).

References

- Breitkopf, P., Naceur, H., Rassineux, A. and Villon, P. (2005), "Moving least squares response surface approximation: formulation and metal forming applications", *Comput. Struct.*, **83**(17-18), 1411-1428.
- Kaltenbacher, M., Kaltenbacher, B., Hegewald, T. and Lerch, R. (2010), "Finite element formulation for ferroelectric hysteresis of piezoelectric materials", *J. Intel. Mat. Syst. Str.*, **21**(8), 773-785.
- Kettil, P. and Wiberg, N.E. (2004), "Simulation of failure of structures using dynamics and optimization techniques", *Comput. Struct.*, **82**(9-10), 815-828.
- Li, T.J. and Wang, Y. (2009), "Performance relationships between ground model and space prototype of deployable space antennas", *Acta Astronaut.*, **65**(9-10), 1383-1392.
- Meguro, A., Shintate, K., Usui, M. and Tsujihata, A. (2009), "In-orbit deployment characteristics of large deployable antenna reflector onboard engineering test satellite VIII", *Acta Astronaut.*, **65**(9-10), 1306-1316.
- Natori, M.C., Takano, T., Inoue, T. and Noda, T. (1993), "Design and development of a deployable mesh antenna for MUSES-B Spacecraft", *Proceedings of the 34th AIAA /ASME /ASCE /AHS /ASC Structures, Structural Dynamics and Materials Conference*, La Jolla, California, AIAA 93-1460.
- Nocedal, J. and Wright, S.J. (2006), *Numerical optimization*, Springer, New York, USA.
- Preumont, A. (2002), *Vibration control of active structures*, Kluwer Academic Publishers, Dordrecht, Netherlands.
- Shi, H. and Yang, B. (2012), *Nonlinear deployable mesh reflectors*, (Eds., Dai, L.M. and Jazar, R.N.), Nonlinear approaches in engineering application, Springer, New York, USA.
- Shultz, G.A., Schnabel, R.B. and Byrd, R.H. (1985), "A family of trust-region-based algorithms for unconstrained minimization with strong global convergence properties", *SIAM J. Numer. Anal.*, **22**(1), 47-67.
- Tabata, M. and Natori, M.C. (1996), "Active shape control of a deployable space antenna reflector", *J. Intel. Mat. Syst. Str.*, **7**(2), 235-240.
- Tabata, M., Yamamoto, K., Inoue, T., Noda, T. and Miura, K. (1992), "Shape adjustment of a flexible space antenna reflector", *J. Intell. Mater. Syst. Struct.*, **3**(4), 646-658.
- Tanaka, H. (2011), "Surface error estimation and correction of a space antenna based on antenna gain analyses", *Acta Astronaut.*, **68**(7-8), 1062-1069.
- Thomson, M. (2002), "Astromesh deployable reflectors for ku and ka band commercial satellites", *Proceedings of the 20th AIAA International Communications Satellite Systems Conference and Exhibit*, Montreal, Canada, AIAA-2002-2032.
- Vassilopoulou, I. and Gantes, C.J. (2010), "Vibration modes and natural frequencies of saddle form cable nets", *Comput. Struct.*, **88**(1-2), 105-119.
- Wang, L., Li, D.X. and Jiang, J.P. (2013), "Mesh topological form design and geometrical configuration generation for cable-network antenna reflector structures", *Struct. Eng. Mech.*, **45**(3), 407-418.
- Wang, Z.W., Li, T.J. and Deng, H.Q. (2014), "Form-finding analysis and active shape adjustment of cable net reflectors with pzt actuators", *J. Aerospace Eng.*, **27**(3), 575-586.
- Yang, B., Shi, H., Thomson, M. and Fang, H. (2008), "Nonlinear modeling and surface mounting optimization for extremely large deployable mesh antenna reflectors", *ASME International Mechanical Engineering Congress and Exposition*, Boston, USA, October 31-November 6.
- You, Z. (1997), "Displacement control of prestressed structures", *Comput. Meth. Appl. Mech. Eng.*, **144**(1-2),

46

Zuwei Wang and Tuanjie Li

51-59.

CC